Int. J. Microgravity Sci. Appl., **33** (1) (2016)330108
DOI: 10.15011/ijmsa.33.330108

IIIII Original Paper IIIII

Flame-Spread Characteristics of n-Decane Droplet Arrays at Different Ambient Pressures in Microgravity

Narita SANO, Naoya MOTOMATSU, Herman SAPUTRO, Takehiko SEO and Masato MIKAMI

Abstract

This research involves microgravity experiments being conducted on flame spread over fuel droplet arrays at different pressures including low-pressure condition in order to improve understanding of flame-spread characteristics under high-altitude relight condition of jet engines. n-Decane was used as a fuel. The ambient pressure ranged from 25 to 200 kPa. The results show that the flame-spread rate and flame-spread-limit distance decreased with an increase in ambient pressure. As the ambient pressure is increased, the thermal conduction time from the flame of a droplet to the next unburned droplet increases due to the decreased thermal diffusivity, and the droplet heating time also increases due to the increased fuel boiling point, resulting in a decrease in the flame-spread rate and -limit distance. The pressure effect on the flame-spread limit around two interactive burning droplets is also discussed.

Keyword(s): Flame Spread, Droplet Array, Pressure Effect, Microgravity
Received 1 Oct. 2015, Accepted 8 Dec. 2015, Published 31 Jan. 2016

1. Introduction

Spray combustion is widely used in gas turbine engines and diesel engines. In order to understand the flame-spread mechanism in fuel sprays, many researchers have conducted microgravity experiments on flame spread of fuel droplet arrays and fuel-droplet clouds. [1-7] Since the droplet diameter is in the order of a few μm in spray combustion, processes occurring in the vicinity of each droplet are not affected by the natural convection in normal gravity. If a relatively large droplet in the order of 1 mmr is used for observation with high resolution in time and space, however, the natural convection affects burning behavior significantly in normal gravity. Therefore, experiments have been carried out in microgravity to suppress the natural convection.

Mikami et al.[4, 7] experimentally investigated the flame-spread-limit distance between droplets at normal pressure and low pressure in microgravity and reported that the flame-spread-limit distance increases as the ambient pressure decreases. Oyagi et al.[5] conducted a flame-spread experiment in microgravity using droplet arrays with uneven droplet spacing and reported that the flame-spread-limit distance increases by two-droplet interactive combustion. Flame-spread experiments of n-decane droplet arrays were conducted in microgravity at pressures of up to 5.0 MPa by Kobayashi et al.[2] The effect of ambient pressure on flame-spread phenomena was investigated. However, the flame spread phenomena including two-droplet interactive combustion at different pressures from low pressure to high pressure have not been reported. This pressure range is important in view of the high-altitude relight of aircraft jet engines. If the jet engine of an aircraft misfires at high altitude, reliable re-ignition must be necessary for flight safety. In this case, the pressure in the combustion chamber is reduced gradually to the ambient pressure with a decrease of the rotational speed of the compressor rotor. The temperature in the combustion chamber decreases as the ambient air comes in. After the successful re-ignition, the chamber pressure and temperature increase again. Although the pressure and temperature in the combustion chamber vary complicatedly, flame-spread researches at different pressures including low-pressure conditions at a constant temperature condition will improve understanding of flame-spread characteristics of fuel droplets under the high-altitude relight conditions of jet engines.

Considering the background described above, this research experimentally investigates the flame-spread of fuel droplet arrays with uneven droplet spacing in microgravity at different pressures including low pressure and high pressure.

2. Experimental Apparatus and Procedure

Figure 1 shows the droplet array with uneven droplet spacing used in this research. Droplet I is the droplet for ignition. Droplets B and A are interactive droplets with droplet spacing of S_{BA}/d_0. Droplet L is the droplet to investigate the flame-spread characteristics. Here, dimensional droplet spacing S is non-dimensionalized by initial droplet diameter d_0.

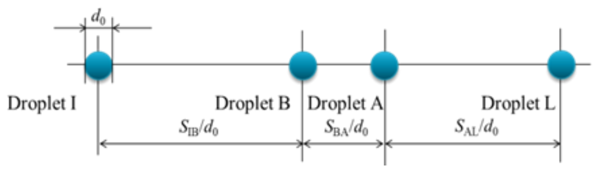

Fig. 1 Droplet array model.

Graduate School of Science and Engineering, Yamaguchi University, 2-16-1 Tokiwadai, Ube, Yamaguchi 755-8611, Japan.
(E-mail: u024ve@yamaguchi-u.ac.jp)

Figure 2 shows the experimental apparatus. Droplets were generated at a designated cross point of 14 µm SiC fibers[3] (Nippon Carbon Hi-Nicalon) by supplying the fuel, n-decane, through a glass needle whose tip inner diameter was about 40 µm. The generated droplet diameter was 0.5 mm at 200 kPa, and 0.75 mm and 0.48 mm[7] at 25 kPa. The glass needle was connected to a motor-driven micro-syringe through a Teflon tube to supply the fuel. The position of the glass needle was controlled by a three-axis traverse system. After generating all the droplets, a digital video camera (SANYO, DMX-FH11) was moved over the droplets. Droplet I was ignited by a hot-wire igniter made of Fe-Cr in microgravity. The droplet spacing between Droplets I and B was $S_{IB}/d_0 = 9$ at 200 kPa and $S_{IB}/d_0 = 18$ at 25 kPa so that heat from the igniter does not affect the other droplets and the interaction between Droplets I and B is negligible. Flame-spread behavior was recorded by a digital video camera with a frame rate of 240 fps. The microgravity experiments were performed at the drop facility of Yamaguchi University, Japan. The microgravity time is 0.95 s. We have added the data at the 25 kPa condition obtained at the 50 m drop tower at the HASTIC Akabira Research Center in the yard of Uematsu Electric Co, Japan. The microgravity time is about 3 s.

The temperature around burning droplets was measured by the thin-filament-pyrometry[6, 8] (TFP) method based on visible radiation from SiC fibers suspending droplets. Since the response time of 14 µm SiC fiber is about 1 ms, the temperature of SiC fiber will closely follows the gas temperature change. Reference 6 showed the TFP method using the same system as in this research is valid for 980 K < T < 1500 K as shown in **Fig. 3**. Considering lower noise in measuring higher temperature by this method, we focus on the 1200 K position in the thermal layer around the burning Droplet A during flame spread.

3. Results and Discussion

3.1 Flame spread of the even-droplet-spacing array

Figure 4 (a) shows direct images of the flame-spread behavior of the fuel-droplet array for $S_{BA}/d_0 = S_{AL}/d_0 = 18.8$ at 25 kPa. **Figure 4 (b)** shows direct images of the flame-spread behavior of the fuel-droplet array for $S_{BA}/d_0 = S_{AL}/d_0 = 10$ at 200 kPa. These values of S/d_0 are near the flame-spread-limit distance for each pressure. In **Fig. 4 (a)**, blue flames were always observed through combustion at 25 kPa. This indicates that soot formation was suppressed. However, at 200 kPa, yellow luminosity from emission of soot was observed and the flame radius was smaller than that in the 25 kPa condition. Elapsed time t/d_0^2 is from the ignition of Droplet B. The initial flames around Droplets A and L were observed at $t/d_0^2 = 0.742$ s/mm^2 and $t/d_0^2 = 1.664$ s/mm^2, and the flame-spread rate between Droplet A and L was calculated as $V_f d_0 = 20.3$ mm^2/s at 25 kPa. On the other hand, the initial flames around Droplets

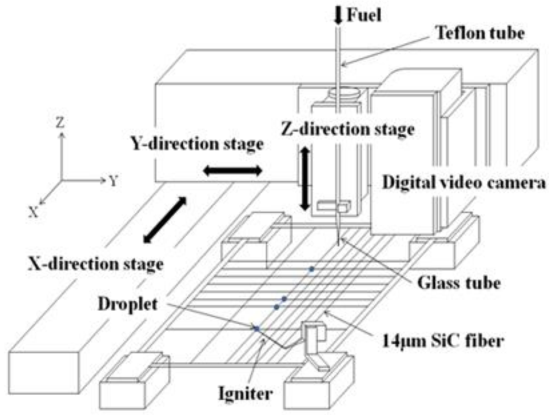

A

Fig. 2 Experimental apparatus.

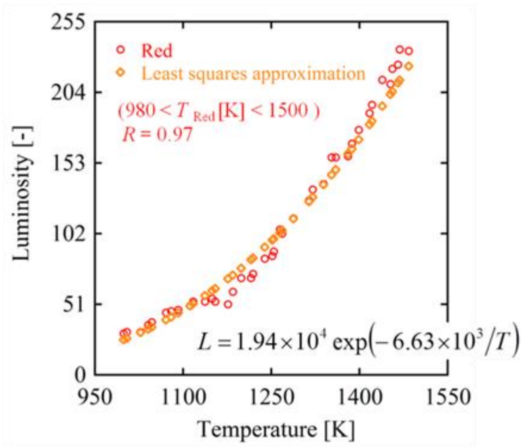

Fig. 3 Relation between R value of heated SiC fiber video image and temperature[6].

$t/d_0^2 = 0.742$ s/mm^2 1.358 s/mm^2 1.664 s/mm^2

(a) $S_{BA}/d_0 = S_{AL}/d_0 = 18.8$ at $P_a = 25$ kPa

$t/d_0^2 = 0.60$ s/mm^2 0.983 s/mm^2 1.083 s/mm^2

(b) $S_{BA}/d_0 = S_{AL}/d_0 = 10$ at $P_a = 200$ kPa

Fig. 4 Burning behavior for droplet arrays with even droplet spacing at different ambient pressures. t/d_0^2 is normalized time from the ignition of Droplet B.

and L were observed at $t/d_0^2 = 0.60$ s/mm^2 and $t/d_0^2 = 0.983$ s/mm^2, and the flame-spread rate between Droplets A and L was calculated as $V_f d_0 = 14.8$ mm^2/s at 200 kPa. The flame-spread rate at 25 kPa was greater than that at 200 kPa although the flame spread limit distance at 25 kPa is larger than that at 200 kPa. In this research, the flame-spread rate was calculated based

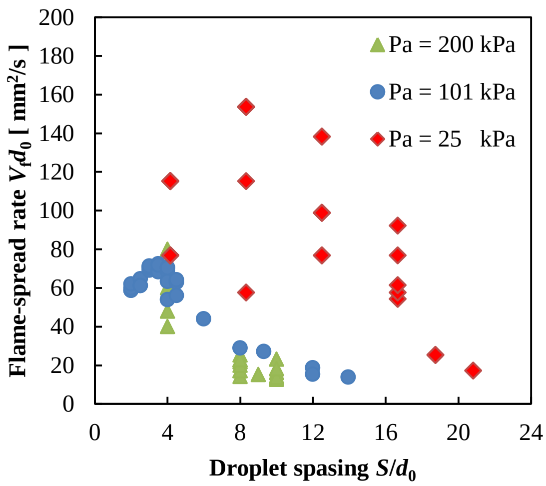

Fig. 5 Flame spread rate $V_f d_0$ on droplet spacing S/d_0 at different ambient pressures. The data for P_a =101 kPa are taken from Ref. 4 and for 25 kPa from Ref. 7.

on the droplet spacing and the flame-spread time between two droplets with a resolution of 1/240 s. The error of flame spread is larger at smaller droplet spacing especially at a lower pressure as discussed in Mikami et al.[7]

Figure 5 shows the dependence of the flame-spread rate on droplet spacing without droplet interaction. The flame-spread rate was normalized by initial droplet diameter d_0 as $V_f d_0$[4]. **Figure 5** suggests that the flame-spread rate increases at the ambient pressure decreases. Since the thermal diffusivity in air decreases and the boiling point of the liquid fuel increases with an increase in ambient pressure, the thermal conduction time from the flame of a droplet to the next unburned droplet increases and the droplet heating time also increases, resulting in a decrease in the flame-spread rate.

3.2 Droplet interaction and local flame-spread-limit distance

Figure 6 (a) shows direct images of the flame-spread behavior of the fuel-droplet array for S_{BA}/d_0 =18 and S_{AL}/d_0 = 22 at 25 kPa. In this condition, the flame cannot spread to Droplet L. **Figure 6(b)** shows direct images of the flame-spread behavior of the fuel-droplet array for S_{BA}/d_0 = 4.2 and S_{AL}/d_0 = 27.1 at 25 kPa. These results suggest that interactive combustion between Droplets B and A increases the flame-spread-limit distance to Droplet L at 25 kPa.

Figures 7(a) and **(b)** show direct images of the flame-spread behavior of the fuel-droplet array for S_{BA}/d_0 = 10 at 200 kPa. In these cases, the droplet spacing between Droplets B and A is close to the flame-spread-limit, therefore, the interaction between Droplets B and A is conceivably negligible. The flame can spread to Droplet L with S_{AL}/d_0 = 10 as shown in **Fig. 7(a)**. However, the flame cannot spread to Droplet L with S_{AL}/d_0 = 12 as shown in **Fig. 7(b)**. From the above, the flame-spread-limit distance exists between S_{AL}/d_0 = 10 and 12. **Figures 7(c)** and **(d)** show direct images of the flame-spread behavior of the fuel-droplet array for S_{BA}/d_0 = 4 at 200 kPa. In the case of S_{BA}/d_0 = 4, the flame can spread to Droplet L with S_{AL}/d_0 = 10 as shown in **Fig. 7(c)** but cannot spread to Droplet L with S_{AL}/d_0 = 12 as shown in **Fig. 7(d)**. These results also suggest that the flame-spread-limit distance for S_{BA}/d_0 = 4 also exists between S_{AL}/d_0

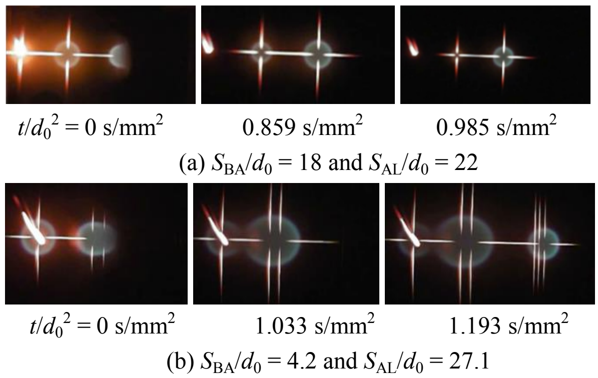

Fig. 6 Burning behavior for droplet arrays with uneven droplet spacing at 25 kPa. t/d_0^2 is normalized time from the ignition of Droplet A.

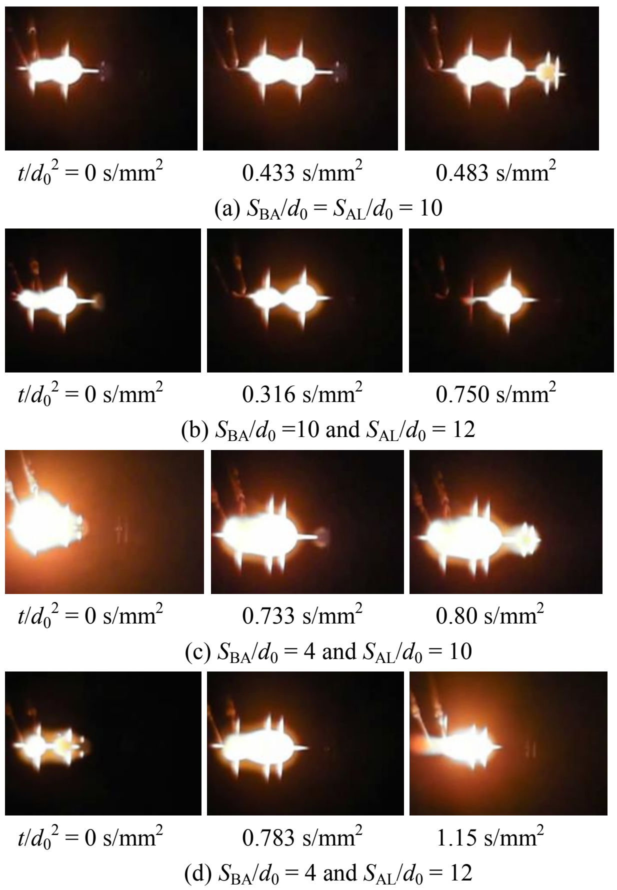

Fig. 7 Burning behavior for droplet arrays with uneven droplet spacing at 200 kPa. t/d_0^2 is normalized time from the ignition of Droplet A.

= 10 and 12 as is suggested in the case of S_{BA}/d_0 = 10 and therefore, the interactive effect in the case of S_{BA}/d_0 = 4 is negligibly small on the flame-spread-limit distance at 200 kPa.

Figure 8 shows the local flame-spread-limit distance of a droplet array with two-droplet interaction between Droplets B and A. The ○ symbol represents droplet spacing S_{AL}/d_0 if flame-spread occurred. The × symbol represents droplet spacing S_{AL}/d_0 if flame spread did not occur at 200 kPa. The ◇ symbol represents droplet spacing S_{AL}/d_0 if flame spread occurred. The + symbol represents droplet spacing S_{AL}/d_0 if flame spread did not occur at 101 kPa taken from Ref. 5. The □ symbol represents droplet spacing S_{AL}/d_0 if flame spread occurred. The △ symbol represents droplet spacing S_{AL}/d_0 if the probability of flame spread occurrence was from 25% to 75%. The Ж symbol represents droplet spacing S_{AL}/d_0 if flame spread did not occur at 25 kPa taken from Ref. 7. In addition, the – symbol represents the same condition added by this research. The flame-spread-limit distance $(S_{AL}/d_0)_{limit}$ exists between ○, ◇, □ and ×, +, Ж. The flame-spread-limit distance increases as the ambient pressure decreases. As for the interactive effect between Droplets B and A, the flame-spread-limit distance increases as S_{BA}/d_0 decreases at 25 kPa, and for S_{BA}/d_0 < 8 at 101 kPa, but stays constant at 200 kPa as shown in **Fig. 8**.

Mikami et al.[7] discussed the reason that the flame-spread-limit distance increases as the ambient pressure decreases in view of the maximum size of the thermal layer around Droplet A. If the droplet spacing is relatively large, flame spread is controlled by thermal diffusion from the flame to the next unburned droplet[4]. We have considered diffusion of heat from the flame surrounding Droplet A to Droplet L in order to investigate the interactive effect of Droplets A and B. **Figure 9** shows temporal variations in the 1200 K position of the thermal layer around Droplet A measured from Droplet A to Droplet L. H_A/d_0 is the leading edge position at 1200 K non-dimensionalized by the initial droplet diameter. At 25 kPa, H_A/d_0 for S_{BA}/d_0 = 4.2 (△ symbol) is greater than that for S_{BA}/d_0 = 18.8 (× symbol) especially between t/d_0^2 = 0.2 s/mm² and 0.7 s/mm². H_A/d_0 is also affected by heat of reaction of fuel vapor from Droplet L even before the ignition of Droplet L. Here, S_{AL}/d_0 = 27.1 for S_{BA}/d_0 = 4.2 and S_{AL}/d_0 = 18.8 for S_{BA}/d_0 = 18.8. The slope of H_A/d_0 becomes larger around t/d_0^2 = 0.8 s/mm² for S_{BA}/d_0 = 4.2 and around t/d_0^2 = 0.5 s/mm² for S_{BA}/d_0 = 18.8. Focusing on the period from 0.2 s/mm² to 0.5 s/mm² when H_A/d_0 was not affected by Droplet L, Fig. 9 suggests that the interaction between Droplets B and A for S_{BA}/d_0 = 4.2 increases the size of the thermal layer around Droplet A at 25 kPa. However, the 1200 K positions of the thermal layer are almost identical for S_{BA}/d_0 = 4 (◇symbol) and S_{BA}/d_0 = 10 (□ symbol) at 200 kPa. These results suggest that the interactive effect on the thermal layer has a pressure dependence and is not significant even for a relatively small droplet spacing of S_{BA}/d_0 = 4 at 200 kPa.

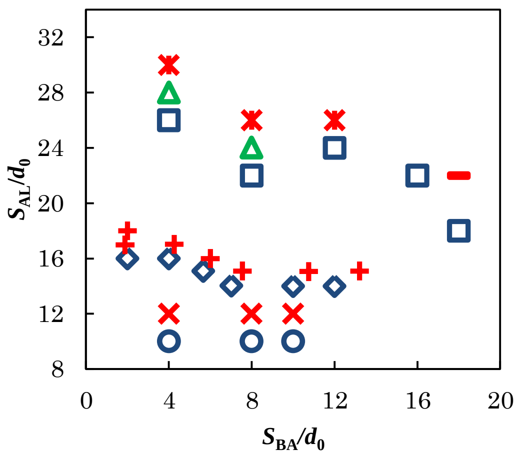

Fig. 8 Dependences of local flame-spread limit distance on the droplet spacing S_{BA}/d_0 for interactive two droplets. The data in the lower part are for 200 kPa, the data in the middle part are for 101 kPa[5], and the data in the upper part are for 25 kPa[7].

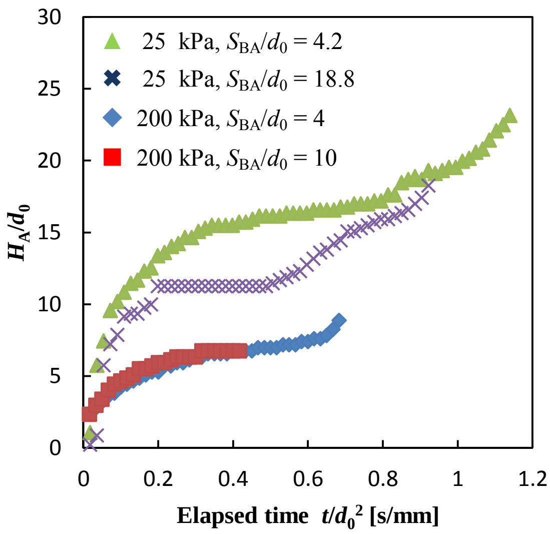

Fig. 9 Temporal variations of thermal layer thickness H_A/d_0 measured from Droplet A for different S_{BA}/d_0 at different pressures.

Mikami et al.[7] showed the maximum radius r_{cmax}/d_0 of temperature T_c in the high-temperature region around a burning droplet as the following equation (1), where, ρ_l is the liquid fuel density, ρ_g is the gas density, H is the fuel heating value, C_p is

$$r_{cmax}/d_0 = \left(\frac{3}{2\pi e}\right)^{1/2}\left\{\frac{\pi\rho_l H}{6\rho_g C_p (T_c - T_a)}\right\}^{1/3} \quad (1)$$

specific heat at constant pressure and T_a is the ambient gas temperature. Since r_{cmax}/d_0 is proportional to the -1/3 power of the ambient pressure, the flame-spread-limit distance is approximated to be proportional to the -1/3 power of the ambient pressure. The flame-spread-limit distance for an n-decane droplet

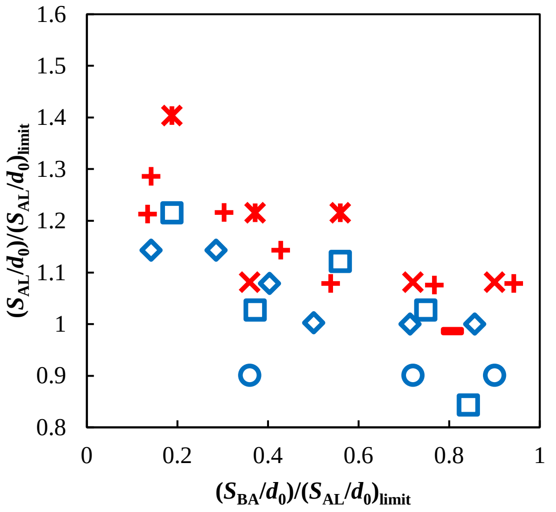

Fig. 10 Flame spread limit distance on droplet spacing between Droplets B and A after normalization by $(S_{AL}/d_0)_{limit}$ at different ambient pressures P_a.

array is $(S/d_0)_{limit}$ = 14.0 at normal pressure in microgravity.[5] Considering this pressure dependence, the flame-spread-limit distance is estimated to be $(S_{AL}/d_0)_{limit}$ = 22.3 at 25 kPa and $(S_{AL}/d_0)_{limit}$ = 11.1 at 200 kPa. **Figure 10** summarizes the results of flame-spread conditions and no-flame-spread conditions in the S_{AL}/d_0-S_{BA}/d_0 plane normalized by $(S_{AL}/d_0)_{limit}$ without droplet interaction. The ○ symbol represents the flame-spread condition at 200 kPa. The × symbol represents the no-flame-spread conditions at 200 kPa. The ◇ symbol represents the flame-spread conditions at 101 kPa.[5] The + symbol represents the no-flame-spread conditions at 101 kPa.[5] The □ symbol represents the no-flame-spread conditions at 25 kPa.[7] The Ж symbol represent the no-flame-spread conditions at 25 kPa taken from Ref. 7. And the – symbol represents the same condition added by this research. **Figure 9** suggests that the normalized flame-spread-limit distance correlates well with $(S_{BA}/d_0)/(S_{AL}/d_0)_{limit}$ considering data scattering at low pressure. The data for symbols □, Ж are taken from Ref. 7 and for symbols ◇ and + are taken from Ref. 5. The – symbol represents the same condition as in Ref. 7 added by this research.

The normalized flame-spread-limit distance increases as $(S_{BA}/d_0)/(S_{AL}/d_0)_{limit}$ decreases. This suggests that the interactive effect can also be understood in the same normalized way. If the droplet spacing between Droplets B and A S_{BA}/d_0 is decreased to sufficiently smaller value than S_{BA}/d_0 = 4, the flame-spread-limit distance could increase even at 200 kPa.

4. Conclusions

This research experimentally investigated the flame-spread-limit distance and flame-spread rate of a fuel droplet array with uneven droplet spacing in microgravity at different ambient pressures.

(1) The flame-spread rate increases as the pressure decreases.

(2) The Flame-spread-limit distance without droplet interaction increases as the pressure decreases.

(3) The flame-spread-limit distance normalized by the flame-spread-limit distance without droplet interaction correlates well with the droplet spacing between two interactive droplets normalized by the flame-spread-limit distance without droplet interaction. This suggests that the interactive effect can also be understood in the same normalized way.

Acknowledgments

We wish to thank Ms. Y. Yoshida and Mr. K. Iwai for their valuable help in experiments. This research was partly subsidized by Grant-in-Aid for Scientific Research (B) (24360350).

References

1) S. Kato, H. Kobayashi and T. Niioka: JSME Int. j., Series B, **41** (1998) 322.
2) H. Kobayashi, J. Park, T. Iwahashi and T. Nioka: Proceedings of the Combustion Institute, **29** (2002) 2603.
3) M. Mikami, H. Oyagi, N. Kojima, M. Kikuchi, Y. Wakashima and S. Yoda: Combustion and Flame, **141** (2005) 241.
4) M. Mikami, H. Oyagi, N. Kojima, M. Kikuchi, Y. Wakashima and S. Yoda: Combustion and Flame, **146** (2006) 391.
5) H. Oyagi, H. Shigeno, M. Mikami, N. Kojima: Combustion and Flame, **156** (2009) 763.
6) M. Mikami, T. Hirose, H. Watari, T. Seo, O. Moriue and M. Kikuchi: 25th European Conference of Liquid Atomization & Spray Systems, (2013) 1014.
7) M. Mikami, N. Sano, H. Saputro, H. Watari and T. Seo: Int. J. Microgravity Sci., **31** (2014) 172 (in Japanese).
8) W.M. Pitts: Proceedings of The Combustion Institute, **26** (1996) 1171.